NANO · MICRO small
www.small-journal.com

Biotransformation and Biological Interaction of Graphene and Graphene Oxide during Simulated Oral Ingestion

Daniela Guarnieri, Paola Sánchez-Moreno, Antonio Esaú Del Rio Castillo, Francesco Bonaccorso, Francesca Gatto, Giuseppe Bardi, Cristina Martín, Ester Vázquez, Tiziano Catelani, Stefania Sabella, and Pier Paolo Pompa**

The biotransformation and biological impact of few layer graphene (FLG) and graphene oxide (GO) are studied, following ingestion as exposure route. An in vitro digestion assay based on a standardized operating procedure (SOP) is exploited. The assay simulates the human ingestion of nanomaterials during their dynamic passage through the different environments of the gastrointestinal tract (salivary, gastric, intestinal). Physical–chemical changes of FLG and GO during digestion are assessed by Raman spectroscopy. Moreover, the effect of chronic exposure to digested nanomaterials on integrity and functionality of an in vitro model of intestinal barrier is also determined according to a second SOP. These results show a modulation of the aggregation state of FLG and GO nanoflakes after experiencing the complex environments of the different digestive compartments. In particular, chemical doping effects are observed due to FLG and GO interaction with digestive juice components. No structural changes/degradation of the nanomaterials are detected, suggesting that they are biopersistent when administered by oral route. Chronic exposure to digested graphene does not affect intestinal barrier integrity and is not associated with inflammation and cytotoxicity, though possible long-term adverse effects cannot be ruled out.

1. Introduction

In the latest years, the interest in graphene has grown continuously toward real applications. Graphene is a single layer of monocrystalline graphite with sp^2-hybridized carbon atoms tightly packed in a 2D honeycomb lattice, resulting in a large surface area on both sides of the planar axis.[1,2] The group of graphene and graphene-related materials (GRMs) comprises, among the others, single-layer graphene, few-layer graphene (FLG), graphene oxide (GO), reduced graphene oxide (RGO), graphene nanosheets, graphene nanoribbons, and graphene quantum dots.[1,3,4] GRMs have distinctive characteristics that make them interesting candidates for technological and biomedical applications, ranging from (opto)electronic to electrochemical devices, energy storage, cell imaging, drug delivery, and biosensors.[3,5–8] Moreover, the use of graphene as nanofiller in food packaging has also been investigated because of its exceptional ability to limit oxygen permeation and light transmission in polymeric films.[9–11]

The integration of GRMs into consumer products makes crucial to assess their potential risk for humans, by defining their toxicological profile and biological fate within the exposed organisms.[12] Exposure to GRMs can mainly occur via inhalation, ingestion, and/or skin contact. Amongst these, inhalation is considered

Dr. D. Guarnieri, Dr. P. Sánchez-Moreno, Dr. F. Gatto, Dr. G. Bardi, Dr. P. P. Pompa
Nanobiointeractions & Nanodiagnostics
Istituto Italiano di Tecnologia (IIT)
Via Morego, 30, 16163 Genova, Italy
E-mail: pierpaolo.pompa@iit.it
Dr. A. E. Del Rio Castillo, Dr. F. Bonaccorso
Graphene Labs
Istituto Italiano di Tecnologia
Via Morego, 30, 16136 Genova, Italy
Dr. F. Gatto
Department of Engineering for Innovation
University of Salento
73100 Lecce, Italy
Dr. C. Martín, Prof. E. Vázquez
Departamento de Química Orgánica
Facultad de Ciencias y Tecnologías Químicas
Universidad de Castilla-La Mancha
13071 Ciudad Real, Spain
Dr. C. Martín, Prof. E. Vázquez
Instituto Regional de Investigación Científica Aplicada (IRICA)
Universidad de Castilla-La Mancha
13071 Ciudad Real, Spain
Dr. T. Catelani
Electron Microscopy Facility
Istituto Italiano di Tecnologia
Via Morego 30, 16163 Genova, Italy
Dr. S. Sabella
Drug Discovery and Development Department
Istituto Italiano di Tecnologia
Via Morego, 30, 16136 Genova, Italy
E-mail: stefania.sabella@iit.it

DOI: 10.1002/smll.201800227

as the most relevant way of GRM entrance in the human body and, hence, several in vitro and in vivo studies have recently focused their attention on this route of exposure.[3,13,14] After inhalation, however, GRMs may also enter the digestive apparatus, through swallowing.[15–17] In addition, unintentional direct ingestion of GRMs could occur from contaminated waters or upon their release from food packaging. Despite such important route of entrance, few works on the fate and toxicological effects of GRMs upon oral exposure have been reported to date.[18–21] Moreover, in vitro models only partially mimic the real in vivo environment, e.g., GRMs directly suspended in cell culture media without previous contact with gastrointestinal (GI) juices[18] or preincubated with acidic buffers that only account for the low pH of the gastric compartment.[19] Therefore, in vitro data are poorly comparable to complex in vivo conditions, including strong pH shifts and variable concentrations of salts and enzymes during ingestion. Hence, a more reliable approach considering all steps occurring after oral ingestion is required for a realistic assessment of biotransformation of GRMs in the GI tract.

As for other nanomaterials,[22–26] the unique physical–chemical characteristics of GRMs may change depending on the surrounding conditions of the biological environment, such as temperature, pH, concentration, salts, and many other factors that, in turn, may influence the interaction of GRMs with biological systems. In this framework, the properties of GRMs may be significantly affected during their passage through the GI tract, due to interaction with the different biological environments (typically composed of complex mixtures of organic and inorganic molecules active in harsh/mild pH conditions), becoming, after the biotransformation, novel species with different characteristics and unknown biological impact. In this respect, some information is available on biotransformation of carbon nanomaterials, including GO and oxidized carbon nanotubes (CNTs), showing that they may be degraded both in vitro and in vivo by oxidase enzymes, such as horseradish peroxidase (HRP) and human myeloperoxidase (hMPO) that are usually present in physiological fluids.[27–29] Notably, detailed knowledge about biotransformation is crucial to address recent regulatory requirements for nanomaterials that suggest a direct relationship between biological transformation/persistence/degradation and/or release of toxic compounds and hazard.[27,28]

To address this issue, we investigated biotransformation/biodurability of FLG and GO in GI fluids upon their in vitro digestion, as well as cell uptake, cytotoxicity, and inflammatory response of these materials. In particular, we used a dynamic in vitro digestion assay, developed to mimic the human ingestion of nanoparticles and monitor their biotransformation during the passage through the GI tract simulated environments (salivary, gastric, intestinal).[24] The assay is part of a standardized operating procedure (SOP)[29] developed in the EU project NANoREG (A common European approach to the regulatory testing of nanomaterials. http://www.nanoreg.eu/). The application of SOPs has the scope to foster data reproducibility by lowering result variability, which often affects the benchmarking analysis among nanomaterials.[30] First, the impact of each step of the in vitro digestion process on the physical-chemical properties of FLG and GO flakes was analyzed by Raman spectroscopy. Second, a thorough cytotoxicological investigation of digested GRMs on an in vitro model of intestinal barrier, a widely adopted test system by pharmacological industries and regulatory authorities,[31] was performed to find a correlation between physical–chemical properties of digested GRMs and cell response. A second NANoREG SOP method was used also for this analysis.[32]

2. Results and Discussion

2.1. Biotransformation of GRMs during the Digestion Process

The in vitro digestion assay adapted for GRM ingestion is schematized in **Figure 1** and described in Table S1 (Supporting Information). This model carefully mimics the gastrointestinal passage and simulates the oral, gastric, and small intestine conditions. To this aim, synthetic digestive juices were used, and all relevant parameters during digestion process such as pH changes, transit times, relevant enzymes, and protein compositions were taken into account, as described previously.[24,33] In this study, FLG and GO flakes were used as model GRMs. FLG flakes were obtained by exfoliation of graphite through interaction with melamine by ball-milling treatment.[34] After exfoliation, melamine was removed by filtration with hot water to obtain stable dispersions of FLG.

Figure 1. Schematic representation of the in vitro digestion assay of GRMs. Along the passage through the different digestive compartments (mouth, stomach, and small intestine), physical–chemical changes of FLG and GO were monitored by Raman spectroscopy. Synthetic digestive juices were used and all relevant parameters during digestion process such as temperature, pH changes, transit times, relevant enzymes, and protein compositions were considered.

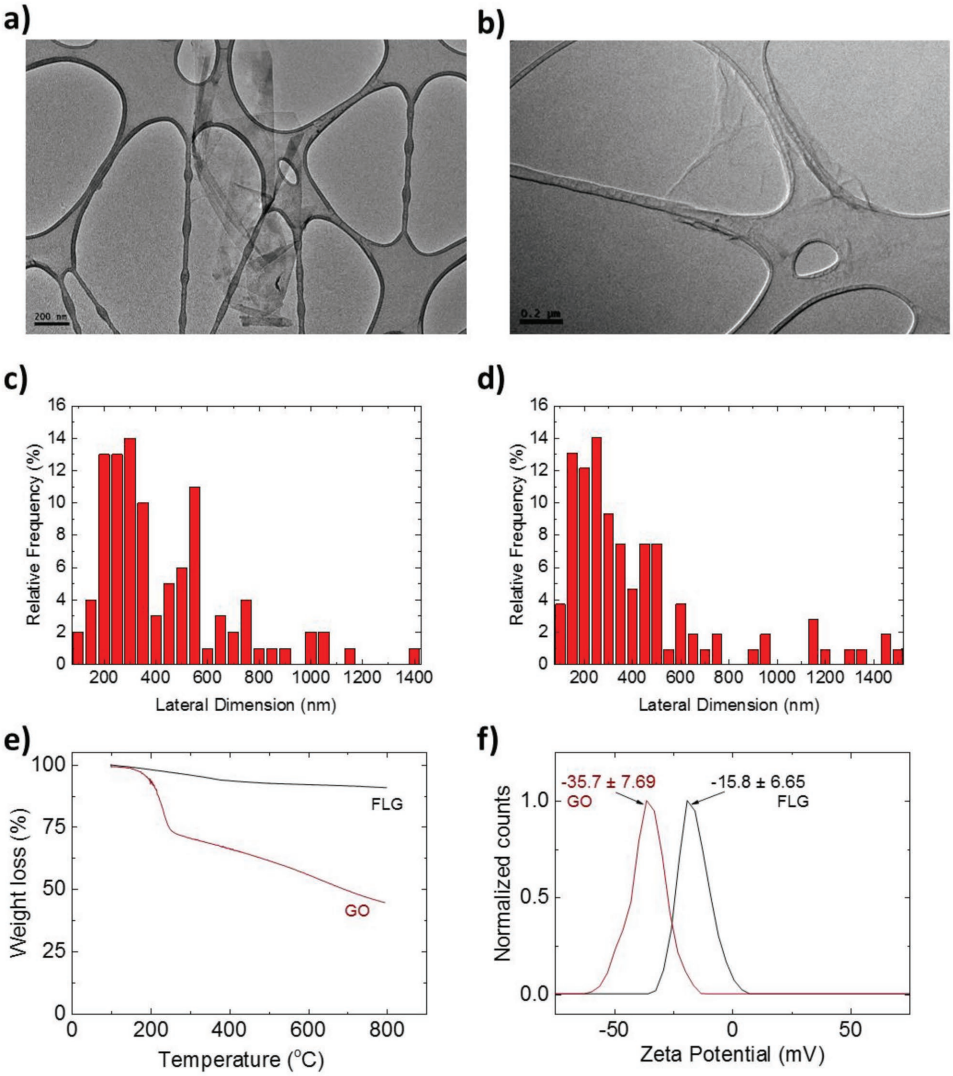

Figure 2. Graphene and graphene oxide characterization. Representative transmission electron microscopy images of a) FLG and b) GO nanosheets. Lateral dimension distribution of c) FLG and d) GO flakes measured by TEM image analysis. e) Thermogravimetric analysis of FLG and GO. f) Zeta-potential of FLG and GO measured at 25 °C and dispersed in MilliQ water.

The final FLG concentration was estimated to be 0.09 mg mL^{-1} with melamine traces (0.09 ppm) as reported elsewhere.[35] GO flakes were obtained through oxidation of carbon fibers (GANF Helical-Ribbon Carbon Nanofibers, GANF). To remove the presence of acids, the initial GO suspensions (concentration <1 mg mL^{-1}) were washed with MilliQ water by centrifugation, at 4000 rpm for 30 min, until a pH value of ≈5 was observed.

The as-prepared GRMs were characterized by transmission electron microscopy (TEM), thermogravimetric analysis (TGA), and Zeta-potential (ζ) in order to gain information about the physical–chemical properties of the starting materials. Representative flakes of FLG and GO, with many visible wrinkles are shown in **Figure 2**a,b, respectively. The statistical analysis of TEM images revealed broad lateral size distributions of both GRMs in water dispersion (Figure 2c,d), in line with previously reported results.[35] The mean flake length was similar for both materials and around 400 nm. Although GO and FLG were very similar in size (Figure 2c,d), TGA experiments were performed to highlight the differences in chemical composition of FLG and GO, i.e., to evaluate quantitatively the oxygenated/functional groups present on both materials. As expected, they revealed large dissimilarities between the two materials, showing a higher amount of oxygenated/functional groups in GO than in FLG. In particular, a weight loss of 8% was obtained for FLG at 600 °C, indicating the low quantity of oxygen groups generated by the exfoliation process, while a weight loss of 46% was observed in the case of GO at the same temperature (Figure 2e). Since FLG and GO were dispersed in MilliQ water to prepare stock suspensions (before dilution into the GI juices), the amount of oxygenated or functional groups could affect directly the stability of the flakes in water. Therefore, we measured Zeta-potential in this dispersant in order to achieve information about the surface charge of the starting

materials. FLG and GO exhibited a surface charge of −20 and −35 mV, respectively (Figure 2f), suggesting a poor stability of FLG and a moderate stability GO in aqueous media, according to the guidelines of the American Society for Testing and Materials.[36] Additionally, the negative ζ were indicative of oxygenated functional groups, present on both FLG and GO flakes.[37]

Depending on their route of entrance into the biological systems, nanomaterials experience different environments that can affect their original physical–chemical properties, e.g., when passing through the stomach, the acids and biological molecules (e.g., enzymes) present in the digestive juices may interact with the functional groups on the FLG or GO surfaces. The changes on the physical–chemical properties of nanomaterials, occurring during the digestion process, have been poorly studied,[19] and they are an important concern that has to be clarified to elucidate the biological impact of such materials. To address this issue, we used Raman spectroscopy analysis to assess the physical–chemical changes of GRMs incubated at specific time intervals in digestive juices, in conditions that mimic the digestion process. Raman spectroscopy has demonstrated to be a powerful tool for the characterization of GRMs, e.g., giving information about doping[38–40] (changing the Fermi surface of graphene, produced electrostatically, chemically or optically), functionalization[41] (covalent bonding of molecules), and oxidation[42,43] of the materials. In general, the Raman spectrum of graphene is characterized by the G peak (≈1580 cm^{-1}), the D peak (≈1350 cm^{-1}), and the 2D peak (≈2680 cm^{-1}). A detailed physical description of the main Raman modes of graphene is reported in the Supporting Information. In particular, Raman spectroscopy is used to identify the type of defects present in graphene (flake edge or in-plane defects, G and D band shapes),[39] doping (G peak position and shape),[39,44–47] and the number of layers (2D band position and lineshape).[44,48] Thus, Raman analysis can provide important information about the possible physical–chemical changes in the graphene flakes, as they go through the simulated digestive tract. **Figure 3** shows representative Raman spectra of the FLG and GO, and the spectra of the simulated digestive juices, i.e., saliva, stomach, and intestine. We can observe the characteristics D, G, D′ and 2D bands for FLG spectra, as well as the typical broad D and G bands, in GO. The Raman spectra of the physiological juices were characterized by two main bands centered at 1450 and 2900 cm^{-1}, attributed to bending and stretching vibrational modes of $-CH_2$ or $-CH_3$, respectively.[49]

To have a general view of the physical–chemical changes of FLG and GO dispersed in biological media, we performed an extensive statistical analysis of the Raman characterization, due to the heterogeneous nature of the FLG and GO. The most significant results are shown in **Figures 4** and **5** and Figure S2 (Supporting Information). In particular, the doping and the change of defects were monitored. Following the evolution of the G band, it was possible to study the doping effects of FLG and GO passing through the simulated digestive tract. The position of the G band has the lowest value when no doping is present in graphene.[42,50–52] The position of the G band—Pos(G)—stiffens as the doping concentration increases[40] and the full width at half maximum of the G band—FWHM(G)—decreases as the doping concentration increases.[51,52] In Figure 4a, the Pos(G) of the FLG (≈1582 cm^{-1}) was maintained

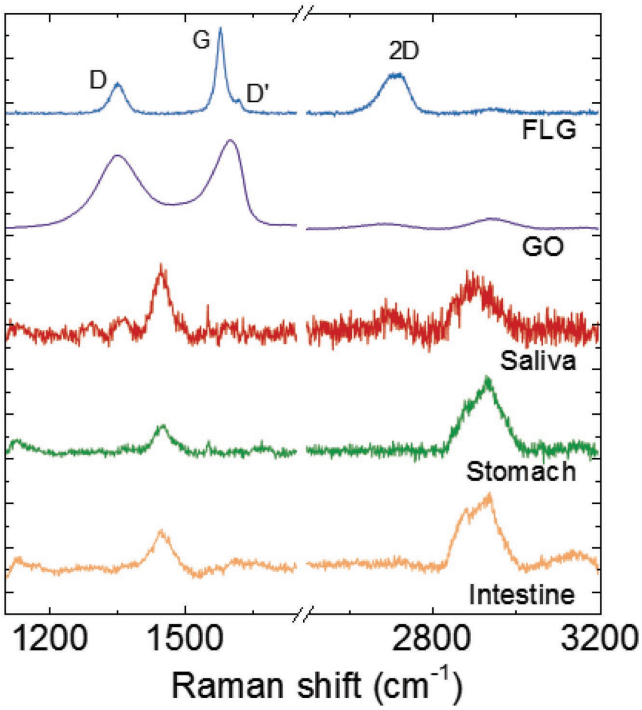

Figure 3. Representative Raman spectra (@514 nm) of GRMs and digestive juices. Few-layers graphene and graphene oxide spectra are reported in blue and purple, respectively. Red, green, and yellow represent Raman spectra of the digestive juices: saliva, stomach, and intestine.

from the starting material (FLG in water), saliva and stomach samples, but in intestine it down-shifts to ≈1580 cm^{-1}. The normal distributions (solid line in the histograms) tended to stiffen gradually when FLG passes from water to intestine. Additionally, the FWHM(G) (Figure 4b) decreased from 22 to 17 cm^{-1}. These two trends, downshifting and stiffening of the G band, indicated that the passing of FLG through the simulated digestive tract gradually incremented the molecules attached on the FLG surfaces (e.g., proteins, salts, and acids), producing a doping effect on the FLG flakes. The defects on graphene flakes, i.e., presence of vacancies, interstitial atoms, and substitutional atoms, were monitored by the D band, specifically the normalized intensity of the D band—$I(D)/I(G)$—and FWHM(D); both these values grow with the number of defects. In Figure 4c, the maximum populations of $I(D)/I(G)$ (in a log-normal distribution[53]) were found at ≈0.3, which was constant for all the samples. This indicates that there was no degradation of FLG. In fact, in the case of degradation, an increase in the $I(D)/I(G)$ ratio should be observed. The standard deviation (σ) did not follow a constant behavior, showing larger values in water and saliva (0.64 and 0.97, respectively), suggesting the aggregation of more flakes in these two compartments. To corroborate the aggregation hypothesis, the stability of FLG flakes at different pH was analyzed by ζ-potential spectroscopy (see also Figure S1, Supporting Information). At low pH values (<5) the FLG was unstable,[54] especially the small flakes (<500 nm), which formed aggregates. On the contrary, at pH 6.5 to 9 the FLG was stable and well dispersed in the media ($\zeta > 30$ mV).[54] Thus, the distribution of $I(D)/I(G)$ for FLG in stomach was

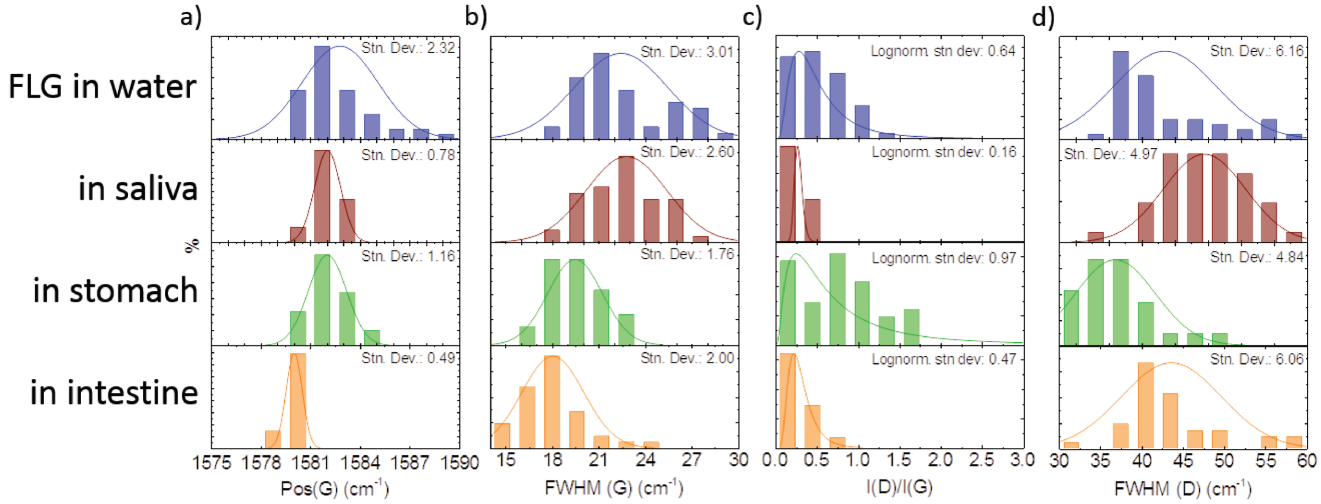

Figure 4. Raman statistical analysis of FLG dispersions in saliva, stomach, and intestine juices. a) Pos(G), b) FWHM(G), c) Normalized intensity $I(D)/I(G)$ and d) FWHM(D) of FLG.

indicative of a collection of flakes aggregated in large clusters, unlike saliva and intestine, where the small flakes were dispersed and homogeneously distributed, and it was possible to observe just large flakes with a strong Raman signal. The FWHM(D) of FLG (Figure 4d) ranged from 32 to 60 cm^{-1}, indicating that the samples were composed by a broad size distribution of the flakes, since FWHM(D) increases inversely with the crystallite size.[55,56] Notably, the FWHM(D) for the FLG dispersed in saliva and intestine had similar distribution to the one of the FLG in water, while in stomach juice the distribution decreased around 35 cm^{-1}, due to the protonation, making a p-type doping of the FLG flakes.[42,50–52]

The 2D subcomponents analysis (Figure S2, Supporting Information) showed no changes in Pos($2D_1$) and Pos($2D_2$). The intensities of the subpeak $2D_1$,—$I(2D_1)/I(G)$—increased from 0.3 to 0.6 when the pH value changed from neutral to acidic (stomach), which led us to conclude that the $2D_1$ intensity was affected by the doping.[40,42] The intensities of the $2D_2$, $I(2D_2)/I(G)$, remained unchanged, as expected, for all the samples, despite the changes in doping.

The GO Raman spectrum is characterized by the G and D bands. Statistical analysis showed that the Pos(G) (≈1580 cm^{-1}) (Figure 5a) remained unchanged for all the samples, while the FWHM(G) distribution became broader in stomach, compared to saliva and intestine, shifting the maximum population from 70 to 100 cm^{-1}. Such broadening of the G band was ascribed to the doping contribution in the stomach, due to the interaction with proteins, salts, and ions,[51] as previously discussed for FLG.

The $I(D)/I(G)$ values of GO were around 1.5 in water, saliva, and stomach, and 1.0 in intestine (Figure 5c). The decrease of the FWHM(D), from 120 cm^{-1} for pristine GO to 90 cm^{-1} in stomach (Figure 5d) was also attributed to the protonation, namely the acid environment made a p-type doping.[42,50–52] For GO in intestine, the FWHM(D) broadened to 110 cm^{-1},

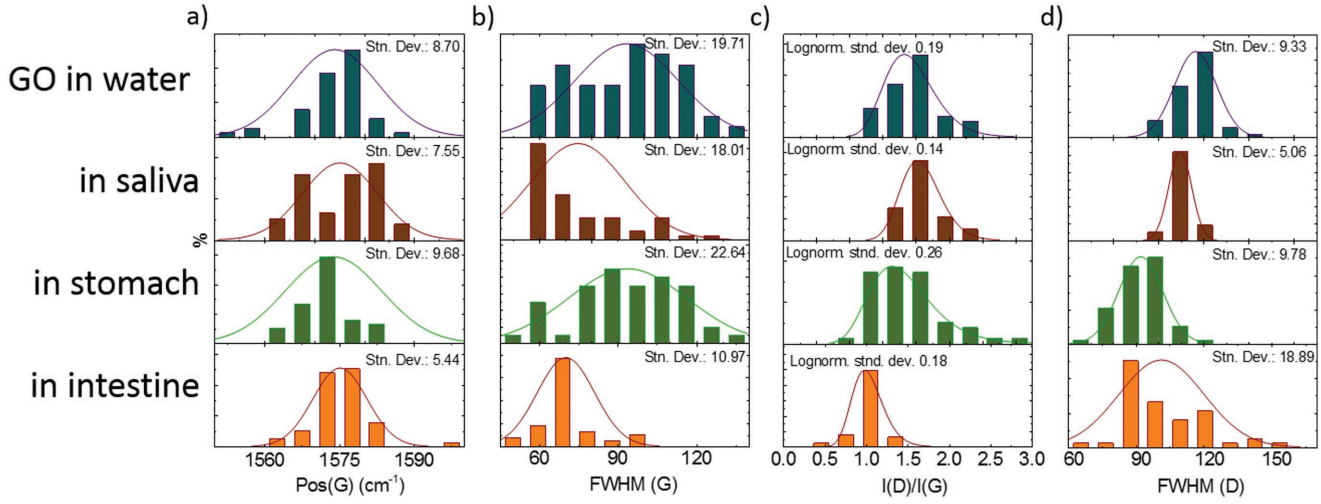

Figure 5. Raman statistical analysis of GO dispersions in saliva, stomach and intestine juices. a) Pos(G), b) FWHM(G), c) Normalized intensity $I(D)/I(G)$ and d) FWHM(D) of GO flakes.

confirming the doping hypothesis. The ζ of GO at different pH is shown in the Figure S1b (Supporting Information).

In summary, Raman analyses indicated that the digestive process did not induce structural defects neither in FLG nor in GO, since no permanent changes were observed in the $I(D)/I(G)$ and FWHM(D) statistics. In addition, the changes of the peaks position (D, G, and 2D), intensity and shape were mainly due to charge changes (doping). This behavior is different from what observed for other nanomaterials.[24,57] For instance, it has been reported that, during digestion, silver nanoparticles are fully dissolved to silver ions that, in turn, interact with the components of digestive juices, forming secondary silver–organic complexes.[24] On the contrary, the Raman results on FLG and GO suggest their aggregation in large clusters in the GI tract. Moreover, the evident interaction with proteins, organic molecules, gastric acids, and salts change the surface chemistry of FLG and GO materials, thus influencing their stability and interaction with the digestive environment.[25,58]

2.2. Assessment of Intestinal Epithelium Integrity upon Chronic Exposure to Digested GRMs

The intestinal barrier is one of the most important biological barriers within the human body. It attends to several functions, such as nutrient uptake, protection against pathogens, and preservation of intestinal microbiome.[59] The impairment of intestinal homeostasis leads to uncontrolled entrance of pathogens and food antigens as well as a dysregulated nutrient supply, which in turn compromise the health of the entire organism. Therefore, as a final step of the digestion process, we tested the biological impact of the digested GRMs on intestinal barrier, to correlate the GRM physical-chemical changes occurring during the digestion process with the cellular response. A reliable in vitro model of intestinal barrier was achieved by growing human intestinal epithelial (Caco-2) cells for 3 weeks on porous inserts (**Figure 6**a) according to a second SOP.[32] Confocal z-sectioning and TEM images showed the formation of a confluent cell layer with the typical structures of intestinal epithelium, such as cell–cell junctions and microvilli (Figure 6b,c). Intestinal barriers were then chronically exposed (up to 9 d) to digested FLG and GO flakes, at the final concentrations of 1 and 5 μg mL^{-1}, respectively. To choose the dose of GRMs, we referred to the human dietary uptake of other nanomaterials. In fact, for silver nanoparticles, concentrations ranging from 1 to 100 μg mL^{-1} were considered to be a realistic dose range in vitro.[57,60,61] Additionally, the used FLG and GO concentrations were selected in order to have the maximum possible concentration allowing good dispersion/stability of the nanomaterials (in particular, the concentration of pristine FLG was lower than GO, due to its worse dispersibility in water solutions).

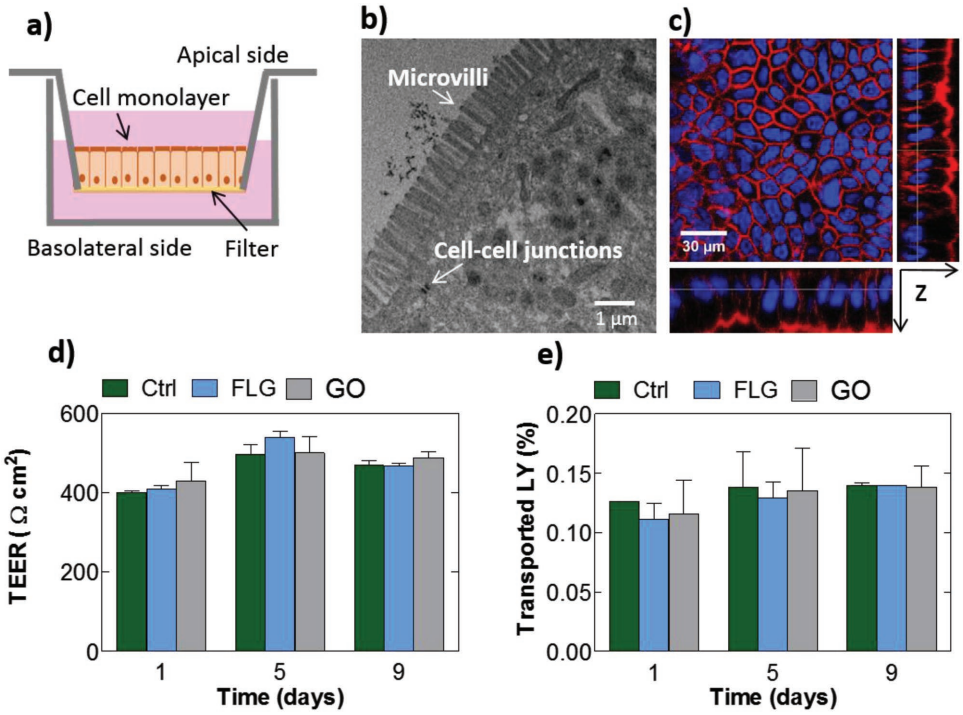

Figure 6. Characterization of the intestinal epithelium formation and integrity after chronic exposure to digested FLG and GO. a) Schematic representation of the intestinal epithelium in vitro model; b) TEM micrograph of 21 d grown intestinal layer showing microvilli and cell–cell junction formation; c) Representative z-sectioning confocal microscopy image of a confluent intestinal layer after 21 d of growth on permeable inserts. Cells were stained with phalloidin (red) and Hoechst 33342 (blue) to highlight actin microfilaments and nuclei. Lateral boxes represent z-stack projections along *x*–*z* and *y*–*z* axis; d) TEER measurements of nontreated control intestinal epithelial layers (Ctrl) and intestinal epithelial layers after 1, 5, and 9 d of chronic exposure to digested FLG and GO; e) percentage of transported LY across the intestinal epithelium after 1, 5, and 9 d of chronic exposure to digested FLG and GO compared with nontreated control intestinal layers (Ctrl). Data represent the average of three different experiments performed in triplicate and the error bars represent the standard deviation. ANOVA and t-test were performed to determine statistical significance.

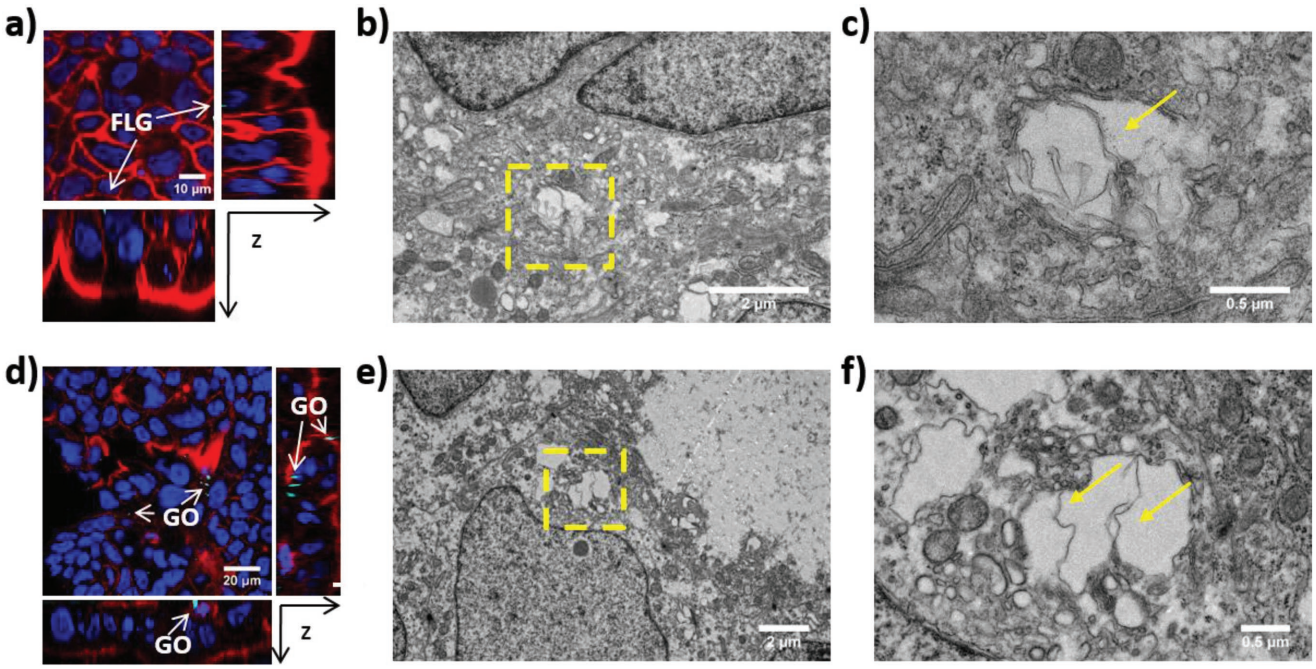

Figure 7. Uptake and intracellular localization of digested FLG and GO nanosheets in Caco-2 intestinal epithelium. Representative z-sectioning confocal microscopy images of confluent intestinal layers after 9 d chronic incubation with digested a) FLG and d) GO. Cells were stained with phalloidin (red) and Hoechst 33342 (blue) to highlight actin microfilaments and nuclei, respectively, and FLG and GO were acquired by reflected light (cyan). Lateral boxes represent z-stack projections along *x*–*z* and *y*–*z* axis. TEM micrographs of digested b,c) FLG and e,f) GO nanoflakes internalized in Caco-2 cell barriers after 9 d chronic incubation. c,f) The zoomed areas highlighted by the yellow dashed squares in (b) and (e), respectively. Yellow arrows indicate GRM flakes.

The integrity of the intestinal layer upon chronic incubation with digested GRMs was assessed by measuring transepithelial electrical resistance (TEER) and passage to the basolateral (Bl) compartment of Lucifer yellow (LY), a marker of paracellular transport (Figure 6d,e). Epithelial layers treated with digested GRMs did not show detectable differences in TEER and LY results with respect to nontreated controls (Figure 6d,e). These results indicated that digested GRMs were well tolerated by the intestinal barrier and did not induce its disruption/perturbation upon chronic exposure. Similar results were also reported by Böhmert et al. after treatment of Caco-2 cell layers with digested silver nanoparticles.[57] In that case, no variations in impedance measurements were observed up to 24 h incubation.

2.3. Cellular Uptake and Intracellular Localization of Digested GRMs

Since digested GRMs did not compromise the integrity of the intestinal barrier, their capability to be internalized by Caco-2 cell layers was investigated by confocal microscopy after 9 d of chronic incubation. As shown in **Figure 7**a,d, very few spots of both FLG and GO were observed within the intestinal layers. Confocal z-sectioning of intestinal epithelia stained with phalloidin and Hoechst confirmed, from a morphological point of view, that the treatment with digested FLG and GO did not affect cell layer integrity and demonstrated the intracellular localization of GRM spots. In our experimental conditions, we observed a limited internalization of GRMs after digestion process, which was likely due to the GRM aggregation when in contact with the components of digestive juices, as suggested by Raman analysis. In fact, we observed large GRM aggregates associated with the intestinal barriers, with a preferential accumulation on the cell membrane, and, sometimes, along cell boundaries (Figure S3, Supporting Information). The size of these aggregates was variable and around some microns (Figure S3, Supporting Information). Another important factor that may reduce the cellular uptake of GRMs was the differentiation status of Caco-2 cells as enterocytes. In fact, it was reported that the undifferentiated Caco-2 cells are more prone than differentiated ones to internalize nanomaterials, such as graphene oxide, quantum dots, TiO_2 and SiO_2 nanoparticles.[21,62–64] In particular, Kucki et al. recently demonstrated that the very dense brush border (made of microvilli) of differentiated intestinal epithelium led to low adhesion of GO sheets and steric hindrance for material uptake.[21] However, a clear understanding of GRM internalization into the cells has not been achieved yet, due to the poor internalization and the difficulty to have comparable in vitro models.[21,65–68] TEM images further confirmed the internalization in Caco-2 cell barriers and suggested a vesicular confinement of internalized digested FLG (Figure 7b,c) and GO (Figure 7e,f). In general, most nanomaterials use endocytosis mechanisms to enter cells and, consequently, they preferentially accumulate into endolysosomes.[23,35,62,69] Therefore, to elucidate the mechanisms of cellular uptake of digested FLG and GO, the lysosomal localization of internalized GRMs within the intestinal barriers was analyzed. Immunofluorescence results indicated the colocalization of digested GRMs

with the lysosomal marker LAMP1, thus suggesting that endocytosis contributed to the internalization of FLG and GO flakes (Figure S4, Supporting Information).

Once localized into the lysosomal compartments, some nanomaterials can undergo degradation, because of the low pH and degradative environment, sometimes causing cytotoxicity due to the release of noxious compounds.[22,23,70] Therefore, because of the lysosomal compartmentalization of digested FLG and GO after cellular uptake, additional studies to assess biocompatibility of GRMs on undifferentiated/proliferating Caco-2 cells were carried out.

Although only differentiated Caco-2 cells represent the epithelial cell layer of the small intestine, immature intestinal cells are also present in the small intestine, due to cell renewal, and they were proved to be more sensitive to external disturbances, e.g., when exposed to silver nanoparticles after in vitro digestion.[57] Therefore, viability and cell membrane integrity of undifferentiated Caco-2 cells were investigated by 3-(4,5-dimethylthiazol-2-yl)-5-(3-carboxymethoxyphenyl)-2-(4-sulfophenyl)-2H-tetrazolium (MTS) and lactate dehydrogenase (LDH) assays, respectively. To this aim, undifferentiated Caco-2 cells were exposed to digested FLG and GO for 2 h every day, up to 4 d. Confocal microscopy images demonstrated the internalization of digested GRMs in Caco-2 cells (Figure S5a, Supporting Information). As expected, the uptake of digested GRMs by undifferentiated Caco-2 cells was significantly higher than intestinal barriers, because, contrary to the latter, undifferentiated Caco-2 cells lacked the typical structures such as tight junctions and microvilli, which hinder nanomaterial internalization.[21,62,63] Despite such higher uptake, both cell viability and cell membrane integrity were not affected by the treatment (Figure S5b,c, Supporting Information). Moreover, treatments with nondigested GRMs, used as controls, further indicated neither significant decrease in cell viability, nor damage of cell membrane (Figure S5b,c, Supporting Information), in line with previously reported data on the same cell type.[18,19] Therefore, lack of cytotoxicity in these cells after exposure to digested GRMs likely suggests no toxicity on intestinal barrier, as well.

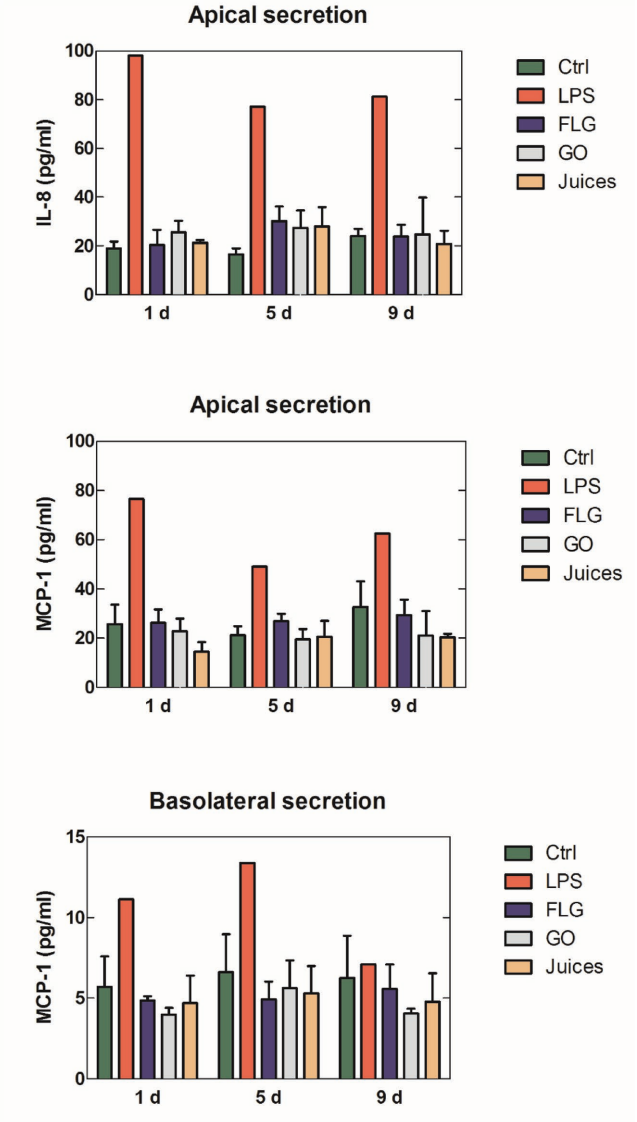

Figure 8. Inflammatory response of Caco-2 intestinal layer upon chronic exposure to digested FLG and GO flakes. Release of IL-8 in apical compartment and MCP-1 in apical and basolateral compartment. Data represent the average of three different experiments performed in triplicate and the error bars represent the standard deviation. ANOVA and t-test were performed to determine statistical significance.

2.4. Inflammatory Response of Intestinal Epithelium to Digested GRMs

In vivo studies on laboratory animals provided some indications that inflammation may be involved in the toxicity of GRMs upon inhalation, and that the extent of inflammatory response could depend on the physical–chemical characteristics (i.e., lateral size, oxidation) of GRMs.[13,14] Therefore, the release of inflammatory cytokines, namely IL-8, MCP-1, IL-1β, IL-6, INFγ, TNFα, MIP1β, and RANTES, in the apical and basolateral media was measured to evaluate the possible triggering of inflammation by the intestinal layers upon chronic exposure to the digested GRMs. Among these, we found the expression of only IL-8 and MCP-1. Caco-2 cell layers usually show a significant increase of IL-8 and MCP-1 levels when stimulated with inflammatory agents.[71–73] In our experiments, the levels of IL-8 and MCP-1 were comparable to untreated cell layers used as negative control (**Figure 8**). On the contrary, positive stimulation with LPS increased the release of the two cytokines (Figure 8). Hence, differently from other nanomaterials,[72] digested GRMs did not induce any significant pro-inflammatory effect on the intestinal epithelium in vitro. A possible explanation for this effect could be related to the larger dimensions of GRMs after digestion, due to aggregation. In particular, GRM aggregates could have different transport rates and be retained outside the cell layer, unlike smaller nanomaterials or ions that may cross the intestinal layer and reach the cells more easily, inducing stronger inflammatory effects. This is consistent with previous findings using Ag nanoparticles, where only smaller 20 nm particles upregulated the IL-8 expression in Caco-2 cell layers, while bigger 100 nm Ag nanoparticles did not.[71,72] Thus, the immobilization of the large GRM aggregates due

to the size-exclusion by the intestinal barrier, could result in a reduced cellular uptake and low cytokine release.

3. Conclusions

In this work, we investigated the biotransformation and biological impact of FLG and GO flakes upon ingestion, by using the NANoREG standard methods simulating in vitro digestion. Our results highlighted the strong influence of digestive juices in modulating the physical–chemical properties of FLG and GO. In particular, the interaction of both GRMs with ions and other molecular components present in digestive juices resulted in evident doping effects and no structural changes. This interaction influenced the aggregation state of FLG and GO with important consequences in bioaccessibility of these materials to the intestinal layer. In fact, digested GRMs were well tolerated by the intestinal barrier up to 9 d of exposure, not inducing detectable damage, even though large GRM aggregates were associated to its apical side. The immobilization of the GRM aggregates, due to the size-exclusion by the typical brush border of the intestinal barrier, resulted in: i) reduced cellular internalization, ii) no short-term cytotoxicity, and iii) low cytokine release. However, because of the observed GRMs biodurability, regardless of the complex and harsh environments they experienced during the digestion simulation and their partial cellular uptake, additional investigations on their long-term fate are necessary in future studies to fully assess their biocompatibility profile.

4. Experimental Section

GRM Synthesis and Characterization: Few layer graphene flakes were prepared by ball-milling pristine graphite, as described elsewhere.[34] Graphene oxide (GO) was provided by Grupo Antolin Ingeniería (Burgos, Spain). GRM morphology and lateral size were analyzed by Jeol JEM 1011 transmission electron microscope (TEM) (Jeol, Japan). Thermogravimetric analysis was carried out using a TGA Q50 (TA Instruments) at 10 °C min^{-1} under nitrogen flow, from 100 to 800 °C. Measurements of Zeta-potential of FLG and GO were carried out with a Zetasizer Nano-ZS (Malvern Instruments, Worcestershire, UK) at 25 °C in MilliQ water. All measurements were performed in triplicate for each sample. All the batches of FLG and GO were tested for the presence of endotoxin by Limulus Amebocyte Lysate (LAL) assay (Pierce, Thermo Scientific) at the concentrations used for the biological experiments. Acceptable and not significant levels of endotoxin (0.043 ± 0.004 EU mL^{-1} for GO and undetectable endotoxin levels for FLG) were found according to US Food and Drug Administration (FDA) guidelines.[74]

In Vitro Digestion Assay: The digestion of GRMs was carried out by an in vitro digestion assay that simulates the human ingestion of nanomaterials. The assay is based on a dynamic model developed by Bove et al.[24] that is also available as a SOP[29] from the European project Nanoreg (NANoREG—A common European approach to the regulatory testing of nanomaterials. http://www.nanoreg.eu/). Briefly, the assay employs artificial juices simulating the human digestive compartments (mouth, stomach, and small intestine), which are dynamically added into the Eppendorf tube under stirring conditions. The assay was slightly modified. The digestive juices were prepared in sterile conditions by combining salt solutions, organic compounds and proteins to obtain the final concentrations in a total reaction volume of 10 mL as reported in Table S1 (Supporting Information). The final pH of each single juice was 6.8 ± 0.1 for saliva, 1.3 ± 0.1 for stomach, 8.1 ± 0.1 for duodenal and 8.2 ± 0.1 for bile. The juices were preheated at 37 °C for at least 2 h before starting the experiments. All chemicals were purchased by Sigma Aldrich.

The assay was conducted following the reported procedure: 20 µL of the FLG and GO dispersions (0.09 and 0.45 mg mL^{-1}, respectively) were added into a 1.5 mL Eppendorf tube. Afterward, the digestive juices were added in a temporal sequence that simulated the transit of food bolus along the gastrointestinal apparatus.[33] To reproduce the mouth compartment, 60 µL of salivary juice at pH 6.8 were mixed with 20 µL of the GRM dispersion and shacked at 37 °C for 5 min. After incubation, 1 µL of the mouth sample was collected and dried on a silicon wafer for Raman spectroscopy analysis (described below). The remaining sample was used to continue the transit into the stomach. To this aim, 120 µL of gastric juice was added to the mouth samples, the pH was adjusted to 2.5 ± 0.5 with 1 M NaOH and the samples were incubated for further 120 min at 37 °C under shaking. At the end of gastric digestion, 1 µL of the stomach samples was processed for the Raman analysis. The remaining samples were employed to simulate digestion in the small intestine, adding to it 120 µL of duodenal fluid, 60 µL of bile salts, and 20 µL of 84.7 g L^{-1} sodium bicarbonate solution and adjusting the pH at 6.5 ± 0.5 with 3.7% HCl. The shaking was stopped after further 120 min of incubation and 1 µL of the samples was dried on a silicon wafer for Raman characterization. For biological experiments with Caco-2 cell layers, the digestion process was carried out in sterile conditions and the digested GRMs were diluted 1:5 in cell culture medium before incubation with the epithelia.

Raman Spectroscopy: 1 µL of dispersion for each sample was drop cast on a Si wafer (LDB Technologies Ltd.) coated with 300 nm of thermally grown SiO_2. The Raman spectra were measured using a Renishaw confocal microscope (514.5 nm laser excitation wavelength with an incident power of ≈1 mW on the sample), with a 50× objective and a grating of 2400 L mm^{-1}. The deposited samples were mapped in rectangular areas of ≈100 µm × 100 µm. The offset between points in the mapping was set to 5 µm. For statistical analysis, 50 spectra of GRMs were randomly selected on each mapping sample. The FLG and GO peaks (D, G, D′, $2D_1$ and $2D_2$) of the selected spectra were fitted with Voigt functions using Origin Pro 2016. All the spectra were normalized to the integral intensity of the G band.

Intestinal Layer Formation and Chronic Treatment with Digested GRMs: Human colon epithelial (Caco-2) cells (gently provided by Dr. Isabella De Angelis, Istituto Superiore di Sanità (ISS), Rome, Italy) were cultured in Dulbecco's modified Eagles Medium (DMEM, Sigma-Aldrich) supplemented with 10% (v/v) fetal bovine serum (FBS, Sigma-Aldrich), 1% nonessential aminoacids (Invitrogen), 100 U mL^{-1} penicillin and 100 mg mL^{-1} streptomycin (Sigma-Aldrich). Cells were maintained in incubator at 37 °C under a humidified controlled atmosphere and 5% CO_2. To obtain intestinal epithelia, cells were seeded in 12-well plates onto porous Millicell hanging cell culture inserts (Merck Millipore) (*d*, 12 mm; *A*, 1.1 cm^2; pore size 0.1 µm) made of polyethylene terephtalate (PET) in 0.5 mL of medium at a seeding density of 1.7 × 10^5 cells per insert in the apical side. 1.5 mL of medium were poured in the basolateral compartment. Cells were grown for 3 weeks, and culture medium was changed every 2 d, to allow the formation of tight junctions and microvilli according to the NANoREG SOP "Standard Operating Procedure for evaluation of NPs impact on Caco2 cell barrier model".[32] Before starting each experiment, transepithelial electrical resistance (TEER) was measured to verify the correct formation of confluent intestinal layers. The cell inserts were then incubated with digested FLG and GO diluted 1:5 in cell culture medium at the final concentrations of 1 and 5 µg mL^{-1}, respectively, for 2 h every 2 d up to 9 d in order to mimic a chronic intestinal exposure. As a control, some cell inserts were incubated with digestive juices without GRMs at the same conditions used for digested materials to verify their possible effect on cell layer integrity and functionality.

Transepithelial Electrical Resistance Measurements: Before and after 1, 5, and 9 d of incubation with digested GRMs, integrity of differentiated Caco-2 cell epithelia were evaluated by TEER using a chop-stick electrodes device (Millicell-ERS voltmeter, Millipore). TEER values were

expressed as Ohms (Ω) $\times$ cm^2 and were calculated according to the following equation

$$\text{TEER} = \left[\Omega \text{ cell monolayer} - \Omega \text{ filter (cell-free)}\right] \times \text{filter area (1.12 cm}^2\text{)} \quad (1)$$

Inserts were considered suitable for experiments if TEER value was > 150 $\Omega \times$ cm^2.

Lucifer Yellow (LY) Assay: At the end of experiments, the impact of digested GRMs on epithelium integrity was evaluated by lucifer yellow (LY, Sigma) assay to determine any difference in this paracellular marker ability to cross the monolayer between GRM-treated inserts and untreated inserts. After 1, 5, and 9 d of incubation with digested GRMs, apical (Ap) and basolateral (Bl) media were collected and cell layers were washed twice with Hanks' Balanced Salt solution (HBSS, Thermo Fisher Scientific). Ap compartment was filled with 0.5 mL of 0.4 mg mL^{-1} LY solution in HBSS and Bl compartment with 1.5 mL HBSS. Cells were then incubated for 2 h at 37 °C. After incubation, 100 µL of the Bl HBSS of each insert (including free cell inserts) were collected and added into a black 96-well plate. LY content was measured by fluorometric detection (ex. 428 nm, em. 536 nm). The percentage of LY passage in Bl side after treatment was compared to the percentage of LY passage in the negative control.

Cell Staining and Confocal Microscopy: After chronic incubation with digested GRMs, cell layers were fixed with 4% paraformaldehyde for 20 min at room temperature, permeabilized with 0.01% Triton ×100 for 5 min and blocked with blocking buffer solution (0.5% bovine serum albumin in PBS) for 20 min. Cells were then stained with 0.1 $\times$ 10^{-9} M Alexa Fluor 594 Phalloidin for 30 min and Hoechst 33342 (Thermo Fisher Scientific) at a concentration of 5 µg mL^{-1} for 5 min, to localize actin microfilaments and cell nuclei, respectively. Confocal microscopy images were acquired by a confocal microscope (Leica TCS-SP5) with an oil-immersion 63× objective, 405, 488, and 561 nm excitation laser wavelengths and a resolution 1024 $\times$ 1024 pixels. Z-sectioning images were acquired with a z-slice thickness of about 0.7 µm.

Transmission Electron Microscopy (TEM): To observe the formation of microvilli and tight junctions as well as the intracellular localization of digested GRMs, the Caco-2 barriers were fixed for 2 h in 1.5% glutaraldehyde in 0.1 M sodium cacodylate buffer (pH 7.4), post fixed in 1% osmium tetroxide in the same buffer and stained overnight with 1% uranyl acetate aqueous solution. The barriers were then dehydrated in a graded ethanol series, infiltrated with propylene oxide and embedded in epoxy resin (Epon 812, TAAB). Semithin and thin sections of the embedded cell monolayer were cut with an ultramicrotome (UC6, Leica) equipped with a diamond knife (Diatome). Images were collected with a Jeol JEM 1011 (Jeol, Japan) electron microscope, operating at an acceleration voltage of 100 kV, and recorded with a 11 Mp fiber optical charge-coupled device (CCD) camera (Gatan Orius SC-1000).

Cytokine and Chemokine Release: Inflammatory cytokine release (panel: IL-8, MCP-1, IL-1β, IL-6, INFγ, TNFα, MIP1β, RANTES) in the apical and basolateral media from the Caco-2 cell layers after 1, 5, and 9 d of chronic treatment with digested GRMs were assessed with a Bio-Plex 1 MAGPIX TM Multiplex Reader (Bio-Rad) according to the manufacturer's procedure. The cells were stimulated with 100 ng mL^{-1} lipopolysaccharide (LPS, from Escherichia coli 0111-B4, Sigma–Aldrich, cat. no. L4391) as positive control.

Supporting Information

Supporting Information is available from the Wiley Online Library or from the author.

Acknowledgements

The authors acknowledge Dr. P. Bove and Dr. C. Carnovale for their help during experiments and the Antolin Group for supporting the commercial material. This project has received funding from the European Union's Horizon 2020 research and innovation program H2020-Adhoc-2014-20 under grant agreement No. 696656—GrapheneCore1 and from the Spanish Ministry of Economy and Competitiveness MINECO (project CTQ2014-53600-R and FEDER fonds).

Conflict of Interest

The authors declare no conflict of interest.

Keywords

biotransformation, digestive juices, graphene, graphene oxide, intestinal barrier

Received: January 18, 2018
Revised: March 13, 2018
Published online: May 14, 2018

[1] P. Wick, A. E. Louw-Gaume, M. Kucki, H. F. Krug, K. Kostarelos, B. Fadeel, K. A. Dawson, A. Salvati, E. Vázquez, L. Ballerini, *Angew. Chem., Int. Ed.* **2014**, *53*, 7714.
[2] A. K. Geim, K. S. Novoselov, *Nat. Mater.* **2007**, *6*, 183.
[3] V. C. Sanchez, A. Jachak, R. H. Hurt, A. B. Kane, *Chem. Res. Toxicol.* **2011**, *25*, 15.
[4] A. Bianco, H.-M. Cheng, T. Enoki, Y. Gogotsi, R. H. Hurt, N. Koratkar, T. Kyotani, M. Monthioux, C. R. Park, J. M. Tascon, *Carbon* **2013**, *65*, 1.
[5] K. Kostarelos, K. S. Novoselov, *Science* **2014**, *344*, 261.
[6] F. Bonaccorso, Z. Sun, T. Hasan, A. Ferrari, *Nat. Photonics* **2010**, *4*, 611.
[7] G. Fiori, F. Bonaccorso, G. Iannaccone, T. Palacios, D. Neumaier, A. Seabaugh, S. K. Banerjee, L. Colombo, *Nat. Nanotechnol.* **2014**, *9*, 768.
[8] F. Bonaccorso, L. Colombo, G. Yu, M. Stoller, V. Tozzini, A. C. Ferrari, R. S. Ruoff, V. Pellegrini, *Science* **2015**, *347*, 1246501.
[9] O. C. Compton, S. Kim, C. Pierre, J. M. Torkelson, S. T. Nguyen, *Adv. Mater.* **2010**, *22*, 4759.
[10] R. Li, C. Liu, J. Ma, *Carbohydr. Polym.* **2011**, *84*, 631.
[11] T. Ramanathan, A. Abdala, S. Stankovich, D. Dikin, M. Herrera-Alonso, R. Piner, D. Adamson, H. Schniepp, X. Chen, R. Ruoff, *Nat. Nanotechnol.* **2008**, *3*, 327.
[12] A. Bianco, *Angew. Chem., Int. Ed.* **2013**, *52*, 4986.
[13] A. Schinwald, F. Murphy, A. Askounis, V. Koutsos, K. Sefiane, K. Donaldson, C. J. Campbell, *Nanotoxicology* **2014**, *8*, 824.
[14] M. Ema, M. Gamo, K. Honda, *Regul. Toxicol. Pharmacol.* **2017**, *85*, 7.
[15] J. Heyder, J. Gebhart, G. Rudolf, C. F. Schiller, W. Stahlhofen, *J. Aerosol Sci.* **1986**, *17*, 811.
[16] W. Yang, J. I. Peters, R. O. Williams, *Int. J. Pharm.* **2008**, *356*, 239.
[17] L. C. Abbott, A. D. Maynard, *Risk Anal.* **2010**, *30*, 1634.
[18] T. H. Nguyen, M. Lin, A. Mustapha, *J. Food Prot.* **2015**, *78*, 996.
[19] M. Kucki, P. Rupper, C. Sarrieu, M. Melucci, E. Treossi, A. Schwarz, V. León, A. Kraegeloh, E. Flahaut, E. Vázquez, *Nanoscale* **2016**, *8*, 8749.
[20] L. De Marzi, L. Ottaviano, F. Perrozzi, M. Nardone, S. Santucci, J. De Lapuente, M. Borras, E. Treossi, V. Palermo, A. Poma, *J. Biol. Regul. Homeostatic Agents* **2013**, *28*, 281.
[21] M. Kucki, L. Diener, N. Bohmer, C. Hirsch, H. F. Krug, V. Palermo, P. Wick, *J. Nanobiotechnol.* **2017**, *15*, 46.
[22] S. Sabella, R. P. Carney, V. Brunetti, M. A. Malvindi, N. Al-Juffali, G. Vecchio, S. M. Janes, O. M. Bakr, R. Cingolani, F. Stellacci, P. P. Pompa, *Nanoscale* **2014**, *6*, 7052.

[23] D. Guarnieri, S. Sabella, O. Muscetti, V. Belli, M. A. Malvindi, S. Fusco, E. De Luca, P. P. Pompa, P. A. Netti, *Nanoscale* **2014**, *6*, 10264.
[24] P. Bove, M. A. Malvindi, S. S. Kote, R. Bertorelli, M. Summa, S. Sabella, *Nanoscale* **2017**, *9*, 6315.
[25] M. P. Monopoli, C. Aberg, A. Salvati, K. A. Dawson, *Nat. Nanotechnol.* **2012**, *7*, 779.
[26] M. Mahmoudi, A. M. Abdelmonem, S. Behzadi, J. H. Clement, S. Dutz, M. R. Ejtehadi, R. Hartmann, K. Kantner, U. Linne, P. Maffre, S. Metzler, M. K. Moghadam, C. Pfeiffer, M. Rezaei, P. Ruiz-Lozano, V. Serpooshan, M. A. Shokrgozar, G. U. Nienhaus, W. J. Parak, *ACS Nano* **2013**, *7*, 6555.
[27] T. Gebel, H. Foth, G. Damm, A. Freyberger, P.-J. Kramer, W. Lilienblum, C. Röhl, T. Schupp, C. Weiss, K.-M. Wollin, *Arch. Toxicol.* **2014**, *88*, 2191.
[28] J. J. Scott-Fordsmand, S. Pozzi-Mucelli, L. Tran, K. Aschberger, S. Sabella, U. Vogel, C. Poland, D. Balharry, T. Fernandes, S. Gottardo, *Nano Today* **2014**, *9*, 546.
[29] S. Sabella, SOP for characterizing MNM fate in biological media and digestive fluids by multi-technique based method, http://www.rivm.nl/en/About_RIVM/International_Affairs/International_Projects/Completed/NANoREG/deliverables/NANoREG_D2_08_SOP_06_For_characterizing_MNM_fate_in_biological_media_and_digestive_fluids_by_multi_technique_based_method.org, **2017**.
[30] E. Valsami-Jones, I. Lynch, *Science* **2015**, *350*, 388.
[31] P. Artursson, J. Karlsson, *Biochem. Biophys. Res. Commun.* **1991**, *175*, 880.
[32] I. De Angelis, Standard Operating Procedure for evaluation of NPs impact on Caco2 cell barrier model, https://circabc.europa.eu/sd/a/fe1ea854-be73-4f58-a2ba-4bc2ce42ee62/SOP%20for%20the%20evaluation%20of%20NMs%20impact%20on%20Caco2%20cell%20barrier%20model%2029052015%20V9.pdf, **2017**.
[33] C. H. Versantvoort, A. G. Oomen, E. Van de Kamp, C. J. Rompelberg, A. J. Sips, *Food Chem. Toxicol.* **2005**, *43*, 31.
[34] V. León, A. M. Rodriguez, P. Prieto, M. Prato, E. Vázquez, *ACS Nano* **2014**, *8*, 563.
[35] M. Bramini, S. Sacchetti, A. Armirotti, A. Rocchi, E. Vázquez, V. L. Castellanos, T. Bandiera, F. Cesca, F. Benfenati, *ACS Nano* **2016**, *10*, 7154.
[36] K. Krishnamoorthy, M. Veerapandian, K. Yun, S.-J. Kim, *Carbon* **2013**, *53*, 38.
[37] J. M. Berlin, A. D. Leonard, T. T. Pham, D. Sano, D. C. Marcano, S. Yan, S. Fiorentino, Z. L. Milas, D. V. Kosynkin, B. K. Price, *ACS Nano* **2010**, *4*, 4621.
[38] L. Yang, X. Jiang, W. Ruan, B. Zhao, W. Xu, J. R. Lombardi, *J. Phys. Chem. C* **2008**, *112*, 20095.
[39] A. C. Ferrari, *Solid State Commun.* **2007**, *143*, 47.
[40] R. Beams, L. G. Cançado, L. Novotny, *J. Phys.: Condens. Matter* **2015**, *27*, 083002.
[41] K. N. Kudin, B. Ozbas, H. C. Schniepp, R. K. Prud'Homme, I. A. Aksay, R. Car, *Nano Lett.* **2008**, *8*, 36.
[42] C. Casiraghi, *Phys. Rev. B* **2009**, *80*, 233407.
[43] A. C. Ferrari, J. Robertson, *Phys. Rev. B* **2000**, *61*, 14095.
[44] A. C. Ferrari, J. Meyer, V. Scardaci, C. Casiraghi, M. Lazzeri, F. Mauri, S. Piscanec, D. Jiang, K. Novoselov, S. Roth, *Phys. Rev. Lett.* **2006**, *97*, 187401.
[45] A. Kaniyoor, S. Ramaprabhu, *AIP Adv.* **2012**, *2*, 032183.
[46] M. Bruna, A. K. Ott, M. Ijäs, D. Yoon, U. Sassi, A. C. Ferrari, *ACS Nano* **2014**, *8*, 7432.
[47] M. Dresselhaus, A. Jorio, S. Filho, A. R. Saito, *Philos. Trans. R. Soc. London, Ser. A* **2010**, *368*, 5355.
[48] D. Graf, F. Molitor, K. Ensslin, C. Stampfer, A. Jungen, C. Hierold, L. Wirtz, *Nano Lett.* **2007**, *7*, 238.
[49] A. Grill, *Annu. Rev. Mater. Res.* **2009**, *39*, 49.
[50] C. Stampfer, F. Molitor, D. Graf, K. Ensslin, A. Jungen, C. Hierold, L. Wirtz, *Appl. Phys. Lett.* **2007**, *91*, 241907.
[51] A. Das, S. Pisana, B. Chakraborty, S. Piscanec, S. Saha, U. Waghmare, K. Novoselov, H. Krishnamurthy, A. Geim, A. Ferrari, *Nat. Nanotechnol.* **2008**, *3*, 210.
[52] S. Pisana, M. Lazzeri, C. Casiraghi, K. S. Novoselov, A. K. Geim, A. C. Ferrari, F. Mauri, *Nat. Mater.* **2007**, *6*, 198.
[53] K. Kouroupis-Agalou, A. Liscio, E. Treossi, L. Ortolani, V. Morandi, N. M. Pugno, V. Palermo, *Nanoscale* **2014**, *6*, 5926.
[54] D. H. Everett, Basic Principles of Colloid Science, The Royal Society of Chemistry, London **1988**.
[55] A. Ferrari, S. Rodil, J. Robertson, *Phys. Rev. B* **2003**, *67*, 155306.
[56] A. Cuesta, P. Dhamelincourt, J. Laureyns, A. Martinez-Alonso, J. M. Tascon, *J. Mater. Chem.* **1998**, *8*, 2875.
[57] L. Böhmert, M. Girod, U. Hansen, R. Maul, P. Knappe, B. Niemann, S. M. Weidner, A. F. Thünemann, A. Lampen, *Nanotoxicology* **2014**, *8*, 631.
[58] G. Duan, S.-g. Kang, X. Tian, J. A. Garate, L. Zhao, C. Ge, R. Zhou, *Nanoscale* **2015**, *7*, 15214.
[59] D. C. Baumgart, A. U. Dignass, *Curr. Opin. Clin. Nutr. Metab. Care* **2002**, *5*, 685.
[60] S. W. Wijnhoven, W. J. Peijnenburg, C. A. Herberts, W. I. Hagens, A. G. Oomen, E. H. Heugens, B. Roszek, J. Bisschops, I. Gosens, D. Van De Meent, *Nanotoxicology* **2009**, *3*, 109.
[61] Y. S. Kim, J. S. Kim, H. S. Cho, D. S. Rha, J. M. Kim, J. D. Park, B. S. Choi, R. Lim, H. K. Chang, Y. H. Chung, *Inhalation Toxicol.* **2008**, *20*, 575.
[62] H. Peuschel, T. Ruckelshausen, S. Kiefer, Y. Silina, A. Kraegeloh, *J. Nanobiotechnol.* **2016**, *14*, 70.
[63] Z. M. Song, N. Chen, J. H. Liu, H. Tang, X. Deng, W. S. Xi, K. Han, A. Cao, Y. Liu, H. Wang, *J. Appl. Toxicol.* **2015**, *35*, 1169.
[64] D. Ye, M. Bramini, D. R. Hristov, S. Wan, A. Salvati, C. Åberg, K. A. Dawson, *Beilstein J. Nanotechnol.* **2017**, *8*, 1396.
[65] Z. Liu, J. T. Robinson, X. Sun, H. Dai, *J. Am. Chem. Soc.* **2008**, *130*, 10876.
[66] H. Yue, W. Wei, Z. Yue, B. Wang, N. Luo, Y. Gao, D. Ma, G. Ma, Z. Su, *Biomaterials* **2012**, *33*, 4013.
[67] S. Zhang, K. Yang, L. Feng, Z. Liu, *Carbon* **2011**, *49*, 4040.
[68] Q. Mu, G. Su, L. Li, B. O. Gilbertson, L. H. Yu, Q. Zhang, Y. P. Sun, B. Yan, *ACS Appl. Mater. Interfaces* **2012**, *4*, 2259.
[69] D. Guarnieri, A. Falanga, O. Muscetti, R. Tarallo, S. Fusco, M. Galdiero, S. Galdiero, P. A. Netti, *Small* **2013**, *9*, 853.
[70] V. De Matteis, M. A. Malvindi, A. Galeone, V. Brunetti, E. De Luca, S. Kote, P. Kshirsagar, S. Sabella, G. Bardi, P. P. Pompa, *Nanomed.: Nanotechnol. Biol. Med.* **2015**, *11*, 731.
[71] T. Stępkowski, K. Brzóska, M. Kruszewski, *Toxicol. In Vitro* **2014**, *28*, 473.
[72] A. Georgantzopoulou, T. Serchi, S. Cambier, C. C. Leclercq, J. Renaut, J. Shao, M. Kruszewski, E. Lentzen, P. Grysan, S. Eswara, *Part. Fibre Toxicol.* **2016**, *13*, 9.
[73] T. Kucharzik, N. Lügering, H. Pauels, W. Domschke, R. Stoll, *Clin. Exp. Immunol.* **1998**, *111*, 152.
[74] C. US FDA, C. CDRH, *ORA*, http://www.fda.gov/Drugs/GuidanceComplianceRegulatoryInformation/Guidances/ucm314718.htm, **2012**.